Biochemical and Biophysical Research Communications 446 (2014) 638–643

Contents lists available at ScienceDirect

Biochemical and Biophysical Research Communications

journal homepage: www.elsevier.com/locate/ybbrc

Crystallographic analysis of NHERF1–PLCβ3 interaction provides structural basis for CXCR2 signaling in pancreatic cancer

Yuanyuan Jiang [a,1], Shuo Wang [a,1], Joshua Holcomb [a], Laura Trescott [a], Xiaoqing Guan [a], Yuning Hou [a], Joseph Brunzelle [b], Nualpun Sirinupong [c], Chunying Li [a,*], Zhe Yang [a,*]

[a] Department of Biochemistry and Molecular Biology, Wayne State University School of Medicine, Detroit, MI, USA
[b] Advanced Photon Source, Argonne National Lab, Argonne, IL, USA
[c] Nutraceuticals and Functional Food Research and Development Center, Prince of Songkla University, Hat-Yai, Songkhla, Thailand

ARTICLE INFO

Article history:
Received 4 March 2014
Available online 15 March 2014

Keywords:
NHERF1
PLCβ3
X-ray crystallography
Scaffold protein
CXCR2
Pancreatic cancer

ABSTRACT

The formation of CXCR2–NHERF1–PLCβ3 macromolecular complex in pancreatic cancer cells regulates CXCR2 signaling activity and plays an important role in tumor proliferation and invasion. We previously have shown that disruption of the NHERF1-mediated CXCR2–PLCβ3 interaction abolishes the CXCR2 signaling cascade and inhibits pancreatic tumor growth in vitro and in vivo. Here we report the crystal structure of the NHERF1 PDZ1 domain in complex with the C-terminal PLCβ3 sequence. The structure reveals that the PDZ1–PLCβ3 binding specificity is achieved by numerous hydrogen bonds and hydrophobic contacts with the last four PLCβ3 residues contributing to specific interactions. We also show that PLCβ3 can bind both NHERF1 PDZ1 and PDZ2 in pancreatic cancer cells, consistent with the observation that the peptide binding pockets of these PDZ domains are highly structurally conserved. This study provides an understanding of the structural basis for the PDZ-mediated NHERF1–PLCβ3 interaction that could prove valuable in selective drug design against CXCR2-related cancers.

1. Introduction

CXC chemokine receptor 2 (CXCR2) is a G protein-coupled receptor that is activated by binding to the chemokine Gro-α, Gro-β, Gro-γ, ENA-78, GCP-2, IL-8, or NAP-2 [1]. CXCR2 mediates neutrophilic migration and plays critical roles in the positioning of oligodendrocyte precursors in developing spinal cord [2–4]. This receptor also functions in angiogenesis and wound healing and contributes to both spontaneous and inflammation-driven tumorigenesis [2,5,6]. Growing evidence suggests that CXCR2 signaling promotes pancreatic cancer progression where its elevated expression correlates with aggressive stages and poor overall prognosis in patients [7,8]. More recent studies indicate that CXCR2 is expressed in various pancreatic ductal adenocarcinoma (PDAC) cell lines and enhances cell proliferation and survival via the autocrine or paracrine effect [9–11]. These findings imply that CXCR2 could be an attractive drug target for developing targeted treatment for pancreatic cancer.

Evidence suggests that CXCR2 interacts directly or indirectly with other receptors, ion channels, transporters, scaffolding proteins, effectors, and cytoskeletal elements to form macromolecular complexes at specialized subcellular domains [4,9]. These dynamic protein–protein interactions regulate CXCR2 signaling function as well as its localization and processing within cells [12,13]. We have shown that CXCR2, phospholipase C-β3 (PLCβ3), and Na^+/H^+ exchanger regulatory factor-1 (NHERF1) form macromolecular complexes at the plasma membrane of pancreatic cancer cells, which functionally couple chemokine signaling to PLCβ3-mediated signaling cascade [9]. PLCβ3, a membrane bound enzyme, catalyzes the formation of inositol 1,4,5-trisphosphate and diacylglycerol from phosphatidylinositol 4,5-bisphosphate. This reaction uses calcium as a cofactor and plays an important role in the intracellular transduction of many extracellular signals [14]. NHERF1 is a PDZ domain-containing protein that typically functions as a scaffold to cluster transporters, receptors, and signaling molecules into supramolecular complexes [15]. We have demonstrated that the formation of the CXCR2–NHERF1–PLCβ3 complex is mediated by NHERF1 PDZ domains, which bridge CXCR2 and PLCβ3 through binding to their C-terminal PDZ-binding motifs [9]. We also showed that disruption of this PDZ-mediated interaction abolishes CXCR2 signaling and inhibits tumor growth in PANC-1 cells and

* Corresponding authors. Address: 540 E. Canfield Street, Detroit, MI 48201, USA. Fax: +1 313 577 2765.
E-mail addresses: cl@med.wayne.edu (C. Li), zyang@med.wayne.edu (Z. Yang).
[1] These authors contributed equally to this work.

http://dx.doi.org/10.1016/j.bbrc.2014.03.028
0006-291X/

also in human PDAC xenograft animal model [9]. These findings imply that targeting the PDZ-mediated CXCR2–PLCβ3 interaction could provide new strategies for therapeutic interventions of CXCR2-related cancers.

In general, PDZ domains mediate protein interactions by recognizing the C-terminal sequence of target proteins and binding to the targets through a canonically and structurally conserved PDZ peptide-binding pocket [16]. The specificity of the interactions is determined mainly by the residues at positions 0 and −2 of the peptides (position 0 referring to the C-terminal residue), whereas other residues do not significantly contribute to the interaction [16]. This has led to the classification of PDZ domains into two major specificity classes: class I, (S/T)X(V/I/L) (X denoting any amino acid); class II, (F/Y)X(F/V/A) [17–19]. However, more recent evidence suggests that PDZ specificity is unexpectedly complex, with the PDZ domain family recognizing up to 7 C-terminal ligand residues and forming at least 16 unique specificity classes [20]. In addition, many PDZ domains can bind to multiple ligands of different peptide classes, and single peptides are capable of binding to distinct PDZ domains [20]. This complex picture raises a challenging problem of how PDZ domains, structurally simple protein-interaction modules, achieve the broad substrate specificity, the nature of which still remains obscure. In this context, we present the crystal structure of NHERF1 PDZ1 in complex with the PLCβ3 C-terminal peptide ENTQL. The structure reveals that the PLCβ3 peptide binds to PDZ1 in an extended conformation with the last four residues making specific side chain contacts. We also show that PLCβ3 can bind both NHERF1 PDZ1 and PDZ2 in PDAC tumor cells, consistent with the observation that the two domains share highly structurally conserved peptide-binding pockets. This study provides the structural basis of the PDZ-mediated NHERF1–PLCβ3 interaction and could be valuable in the development of novel therapeutic strategies against aggressive pancreatic cancers.

2. Materials and methods

2.1. Protein expression and purification

For X-ray crystallography, a DNA fragment encoding the human NHERF1 PDZ1 (residues 11–94) was amplified by PCR using the full-length human NHERF1 cDNA as a template. The C-terminal extension ENTQL that corresponds to residues 1230–1234 of human PLCβ3 was created by inclusion of 15 extra bases in the reverse primer. The PCR products were cloned in the pSUMO vector containing an N-terminal His6-SUMO tag. The resulting clone was transformed into *Escherichia coli* BL21 Condon Plus (DE3) cells for protein expression. The transformants were grown to an OD600 (optical density at 600 nm) of 0.4 at 37 °C in LB medium, and then induced with 0.1 mM isopropylthio-β-D-galactoside at 15 °C overnight. The cells were harvested by centrifugation and lysed by French Press. The soluble fraction was then subjected to Ni^{2+} affinity chromatography purification, followed by the cleavage of the His6-SUMO tag with yeast SUMO Protease 1. PDZ1 proteins were separated from the cleaved tag by a second Ni^{2+} affinity chromatography and further purified by size-exclusion chromatography. Finally, the proteins were concentrated to 30–40 mg/ml in a buffer containing 20 mM Tris–HCl (pH 8.0), 150 mM NaCl, 1 mM β-mercaptoethanol, and 5% glycerol. For pulldown experiments, glutathione S-transferase (GST) fusion proteins were generated by cloning NHERF1 PDZ1 (1–97), PDZ2 (133–244), or PDZ1–PDZ2 (1–244) into the pGEX4T-1 vector [4]. His-S-tagged proteins were generated by cloning PLCβ3 C-terminal fragment (residues 1135–1234) into the pET30 vector [9]. GST–PDZ proteins were purified using glutathione agarose beads (BD Biosciences) and eluted with 50 mM glutathione. His-S-PLCβ3 was purified using Cobalt resins (Thermo Scientific) and eluted with 200 mM imidazole.

2.2. Crystallization, data collection and structure determination

Crystals were grown by the hanging-drop vapor-diffusion method by mixing the protein (~25 mg/ml) with an equal volume of a reservoir solution containing 100 mM sodium acetate, pH 4.6, 2.5 M sodium chloride at 20 °C. Crystals typically appeared overnight and continued to grow to their full size in 3–4 days. Prior to X-ray diffraction data collection, crystals were cryoprotected in a solution containing the mother liquor and 25% glycerol and flash cooled in liquid nitrogen. The data were collected at 100 K at beamline 21-ID-F at the Advanced Photon Source (Argonne, IL) and processed and scaled using the program XDS [21]. Crystals belong to the space group $P3_121$ with unit cell dimensions $a = b = 50.7$ Å, $c = 66.7$ Å, and one molecule in the asymmetric unit (Table 1). The structure was solved by the molecular replacement method with the program PHASER [22] using the PDZ1–CXCR2 structure (PDB code: 4JL7) as a search model. Structure modeling was carried out in COOT [23], and refinement was performed with PHENIX [24]. To reduce the effects of model bias, iterative-build OMIT maps were used during model building and structure refinement. The final

Table 1
Crystallographic data and refinement statistics.

Data	
Space group	$P3_121$
Cell parameters (Å)	
a, b	50.7
c	66.7
Wavelength (Å)	1.1272
Resolution (Å)	33.3–1.47 (1.51–1.47)
R_{merge}[a]	0.041 (0.575)[b]
Redundancy	6.9 (6.5)
Unique reflections	17,247
Completeness (%)	99.5 (100)
$\langle I/\sigma \rangle$	21.2 (2.7)
Refinement	
Resolution (Å)	26.6–1.47 (1.52–1.47)
Molecules/AU	1
R_{work}[c]	0.181 (0.276)
R_{free}[d]	0.196 (0.325)
Ramachandran plot	
Residues in favored	98.9%
Residues in allowed	1.1%
RMSD	
Bond lengths (Å)	0.005
Bond angels (°)	0.95
No. of atoms	
Protein	1334
Peptide	80
Water	93
Chloride	4
Nickel	1
B-factor (Å^2)	
Protein	37.5
Peptide	41.2
Water	42.7
Chloride	37.7
Nickel	41.0

[a] $R_{merge} = \sum|I - \langle I \rangle|/\sum I$, where I is the observed intensity and $\langle I \rangle$ is the averaged intensity of multiple observations of symmetry-related reflections.
[b] Numbers in parentheses refer to the highest resolution shell.
[c] $R_{work} = \sum|F_o - F_c|/\sum|F_o|$, where F_o is the observed structure factor, F_c is the calculated structure factor.
[d] R_{free} was calculated using a subset (5%) of the reflection not used in the refinement.

models were analyzed and validated with Molprobity [25]. All figures of 3D representations of the PDZ1–PLCβ3 structure were made with PyMOL (www.pymol.org).

2.3. Cell culture

Human PDAC cell lines (PANC-1, AsPC-1, and BxPC-3) were obtained from American Type Culture Collection (Manassas, VA). Cells were cultured in Dulbecco's modified Eagle's medium (Thermo Scientific Hyclone) containing 4.5 mg/ml D-glucose and L-glutamine supplemented with 10% FBS, 100 units/ml penicillin, and 100 μg/ml streptomycin at 37 °C in humidified air with 5% CO_2.

2.4. Pulldown assays

GST pulldown assays were preformed as previously described [4]. Briefly, PDAC cells were lysed in a binding buffer containing phosphate-buffered saline (PBS), 0.2% Triton X-100, and a mixture of protease inhibitors. Supernatant was equally mixed with GST alone or various GST–PDZ fusion domains (GST–PDZ1, GST–PDZ2, or GST–PDZ1–PDZ2) at 4 °C for 2 h. The mixture was pulled down by glutathione agarose beads at 4 °C overnight, washed three times with the binding buffer, and then eluted in Laemmli sample buffer containing β-mercaptoethanol. The eluents were separated by SDS–PAGE and immunoblotted with anti-PLCβ3 antibody. To verify the direct NHERF1–PLCβ3 interaction, purified GST-NHERF1 PDZ domains or GST alone were mixed with a purified His-S-PLCβ3 C-terminal fragment (last 100 residues) in the binding buffer at 20 °C for 1 h. The mixtures were incubated with glutathione agarose beads for 2 h. The beads were washed three times with the binding buffer and eluted with Laemmli sample buffer containing β-mercaptoethanol. The eluents were resolved by SDS–PAGE and probed with S-protein HRP conjugate (for detection of S-tag fusion proteins; EMD Millipore Bioscience). All experiments were repeated at least three times, and the results were consistent.

2.5. Protein data bank accession number

Coordinates and structure factors have been deposited in the Protein Data Bank with accession number 4PQW.

3. Results and discussion

3.1. Binding specificity of NHERF2–PLCβ3 interaction

The overall structure of NHERF1 PDZ1 is similar to other PDZ domains [19,26], consisting of six β strands (β1–β6) and two α-helices (αA and αB) (Fig. 1A and B). The PLCβ3 peptide binds in the cleft between β2 and αB, burying a total solvent-accessible surface area of 381.8 Å^2. The binding specificity of the PDZ1–PLCβ3 interaction is achieved through networks of hydrogen bonds and hydrophobic interactions (Fig. 1C). At the ligand position 0, the side chain of Leu0 is nestled in a deep hydrophobic pocket formed by invariant residues Tyr24, Phe26, and Leu28 from β2 and Val76 and Ile79 from αB (Fig. 1D). In the pocket, the position of Leu0 is further secured by both a hydrogen bond from its amide nitrogen

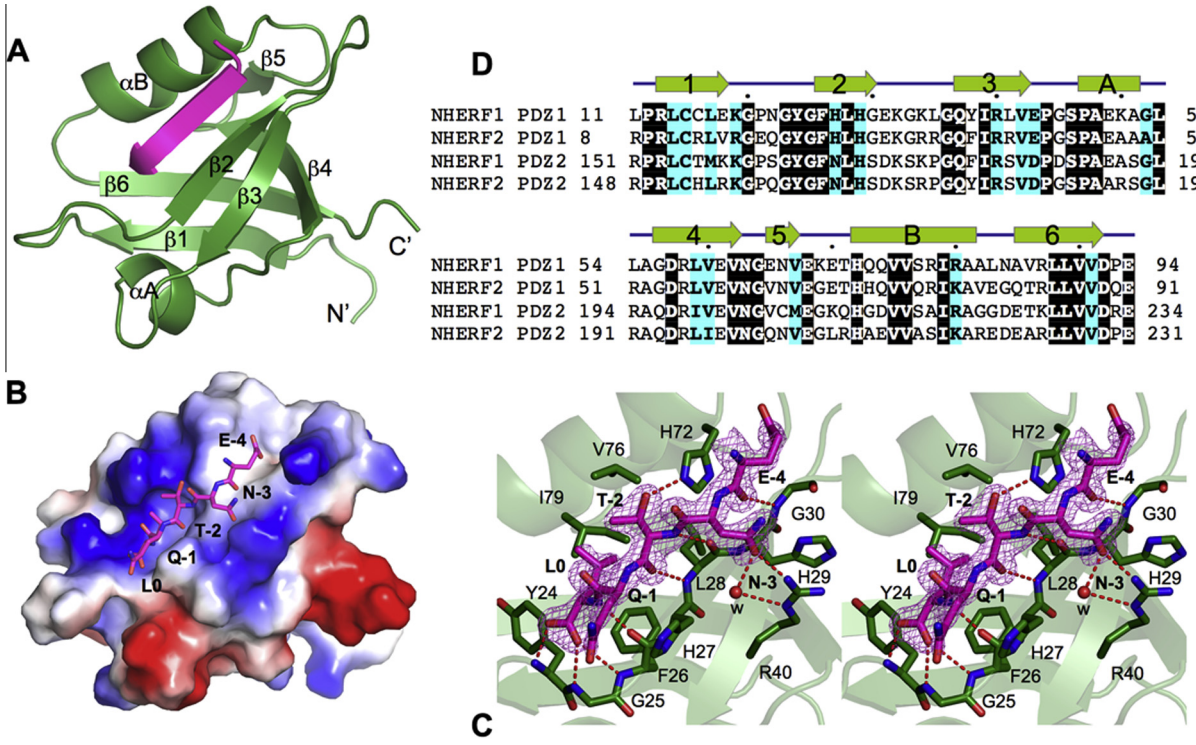

Fig. 1. Structure of NHERF1 PDZ1 in complex with the PLCβ3 C-terminal sequence ENTQL. (A) Ribbon diagram of the PDZ1–PLCβ3 structure. PDZ1 is shown in green and the PLCβ3 peptide is shown in magenta. Secondary structures of PDZ1, α-helices, and β-strands are labeled and numbered according to their position in the sequence. (B) Surface representation of the PDZ1–PLCβ3 structure. Surface coloring is according to the electrostatic potential: red, white, and blue correspond to negative, neutral, and positive potential, respectively. The vacuum electrostatics/protein contact potential was generated by PyMOL. The PLCβ3 peptide is depicted by sticks. (C) Stereo view of the PDZ1 ligand-binding site bound to the PLCβ3 C-terminal peptide. PDZ1 residues are represented by sticks with their carbon atoms colored in green. The PLCβ3 peptide is depicted by sticks overlaid with $2F_o - F_c$ omit map calculated at 1.47 Å and contoured at 1.8σ. Hydrogen bonds are illustrated as red broken lines. (D) Sequence alignment of selected PDZ domains. The alignment was performed by ClustalW [30], including human NHERF1 and NHERF2. Identical residues are shown as white on black, and similar residues appear shaded in cyan. Secondary structure elements are displayed above the sequences and labeled according to the scheme in A. Sequence numbering is displayed to the left of the sequences, with every 10th residue marked by a dot shown above the alignment. (For interpretation of the references to color in this figure legend, the reader is referred to the web version of this article.)

to the Phe26 carbonyl oxygen and triplet hydrogen bonding between the Leu0 carboxylate and the amides of Tyr24, Gly25, and Phe26. Similar interactions have been observed in several other PDZ-mediated complexes [19,26], which represent the most-conserved binding mode for terminal Leu recognition.

Residues at other peptide positions also contribute to the PDZ1–PLCβ3 complex formation (Fig. 1C). At the ligand position −1, the aliphatic portion of the Gln-1 side chain makes Van der Waals interaction with the imidazole ring of His27. At position −2, Thr-2 makes one hydrogen bond to the His72 imidazole group and two hydrogen bonds to the highly conserved residue Leu28. At the ligand position −3, the interactions with Asn-3 include a direct hydrogen bond from its side chain oxygen to the Nη1 atom of Arg40 and a water-mediated hydrogen bond to the Nε atom of Arg40. The latter two interactions represent ligand specific interactions, as the small side chain of Ser-3 is recognized by His29 in PDZ1–CXCR2 complex [27,28]. Finally, the peptide residue Glu-4 engages in a main chain contact with Gly30, but does not participate in any specific side chain interactions. These observations indicate that the last four residues of PLCβ3 contribute to the binding specificity in the PDZ1–PLCβ3 complex formation.

3.2. Endogenous PLCβ3 interacts with both NHERF1 PDZ1 and PDZ2

To gain further insight into the NHERF1–PLCβ3 interaction, we performed GST pulldown assays to examine whether NHERF1 PDZ domains interact with endogenous PLCβ3 in PDAC cells. Lysates of various PDAC cells, PANC-1, AsPC-1, and BxPC-3 were used to interact with the GST fusion proteins GST–PDZ1, GST–PDZ2, and GST–PDZ1–PDZ2. As shown in Fig. 2A, no PLCβ3 was detected in the control lane containing GST alone, but significant amounts of PLCβ3 were found in the lanes containing PDZ1, PDZ2, and both PDZ domains together. Similar results were observed for all PDAC cell lines tested in our experiments. To check whether the PDZ–PLCβ3 interaction is direct, we performed GST pulldown assays with a purified peptide corresponding to the last 100 amino acids of PLCβ3. We observed similar binding results where PLCβ3 interacts with both PDZ domains of NHERF1 (Fig. 2B and C).

To understand the structural basis of the bivalent binding, we performed a structural alignment between the structure of NHERF1 PDZ1 and the structure of NHERF1 PDZ2. The alignment reveals that NHERF1 PDZ1 and PDZ2 share highly similar overall structures and highly conserved ligand-binding pockets (Fig. 3). The root mean square (rms) difference is 1.35 Å for the overall structure (86 Cα atoms), and for the ligand-interacting residues, 0.44 Å. The only notable difference in the ligand-binding sites is residue 27, which is His in PDZ1 and Asn (residue 164) in PDZ2. It should be noted that this conserved substitution maintains the amino functionality of the side chain, which is not expected to disrupt the observed Van der Waals contact between PDZ1 and PLCβ3 (Fig. 1C). Therefore, the comparison of PDZ1 and PDZ2 provides a structural explanation for the ability of PLCβ3 to bind to both PDZ domains.

3.3. Implication in selective drug design

We previously have suggested that targeting the NHERF1-mediated CXCR2–PLCβ3 interaction may have a therapeutic potential in PDAC treatment, as inhibition of this interaction has been found to be sufficient to inhibit CXCR2 signaling activity both in vitro and in vivo [9]. These findings highlight the significance of our present structure studies, and imply that structural details of the NHERF1–PLCβ3 interaction may be valuable in developing new methods and strategies for selective drug design. For instance, this information can be used to create new NHERF1 inhibitors that are potent and specific to block the NHERF1–PLCβ3 interaction. Such inhibitors have the potential to inhibit pancreatic tumor growth by suppressing CXCR2 signaling, and preventing tumor cell proliferation and invasion. In addition, the ability of PLCβ3 to bind both PDZ domains (Fig. 2), together with similar PDZ structures (Fig. 3), suggests NHERF1 inhibitors may be capable of targeting PDZ1 and PDZ2 simultaneously. Such inhibitors might be advantageous in cancer treatment, as PDZ1 and PDZ2 have been shown to have differential roles during metastasis. NHERF1 PDZ2 promotes visceral metastasis via invadopodia-dependent invasion and anchorage-independent growth, as well as by inhibition of apoptosis; while PDZ1 promotes bone metastasis by stimulating podosome nucleation, motility, angiogenesis, and osteoclastogenesis in the absence of increased growth or invasion [29]. It is conceivable that simultaneous targeting of the PDZ domains could lead to a combinatorially synergetic effect that would prevent metastatic behavior and inhibits mesenchymal-to-vasculogenic phenotypic transition in cancer patients. While the biological impact of the bivalent NHERF1–PLCβ3 interaction is currently unknown, future studies should be directed toward evaluation of its effect on CXCR2-mediated PDAC proliferation and invasion, and especially

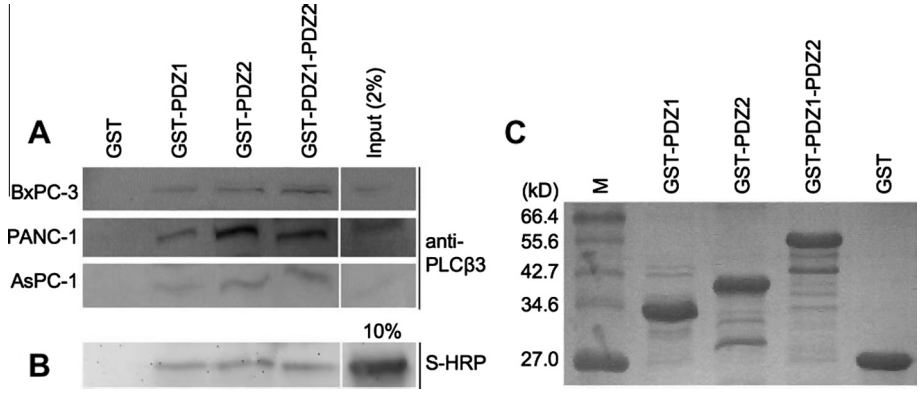

Fig. 2. Endogenous PLCβ3 in human pancreatic cancer cells interacts with both NHERF1 PDZ1 and PDZ2. (A) GST pull-down of endogenous PLCβ3 with NHERF1 PDZ domains. Lysates of PDAC cells, BxPC-3, PANC-1, or AsPC-1 were used as prey. GST fusion proteins of NHERF1 PDZ1, PDZ2, or PDZ1–PDZ2 were used as bait. GST alone served as a negative control. Binding experiments were analyzed by SDS–PAGE and visualized by immunoblotting using anti-PLCβ3 antibody. (B) GST pull-down assays to detect direct interaction between purified PLCβ3 and NHERF1. A His-S-tagged peptide corresponding to the last 100 residues of PLCβ3 was used as prey. Purified GST–PDZ1, GST–PDZ2, GST–PDZ1–PDZ2, or GST alone was used as bait. Binding was resolved by SDS–PAGE and detected with S-HRP conjugate. (C) SDS–PAGE analysis of beads-immobilized GST proteins in each above reaction (loading control). Lane M is molecular weight markers. Molecular weights are indicated at the left of the gel. The gel is visualized by Coomassie blue staining.

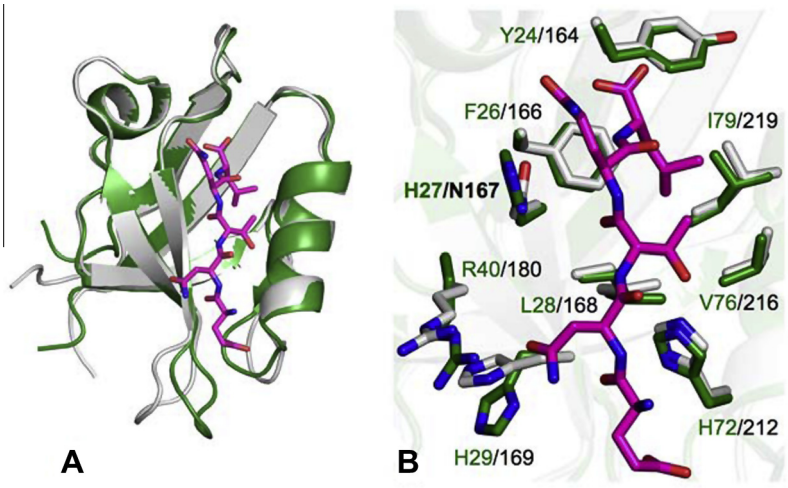

Fig. 3. Structural comparison of NHERF1 PDZ1 and PDZ2. (A) Superposition of the structures of PDZ1–PLCβ3 (green; PDB code: 4PQW) and PDZ2 (gray; PDB code: 2OZF). PDZ domains are represented by ribbons. Residues in PLCβ3 are displayed as sticks with the carbon atoms shown in magenta. (B) Superposition of the PDZ ligand binding pockets. Both PDZ and ligand residues are depicted by sticks and colored according to the scheme in A. (For interpretation of the references to color in this figure legend, the reader is referred to the web version of this article.)

toward determining whether different PDZ domains could mediate the assembly of distinct CXCR2 signal transduction complexes. Such studies should have important implications in specific NHERF1 scaffolding regulation and also in many CXCR2-associated human cancers.

Acknowledgments

This study was supported by the Leukemia Research Foundation, Aplastic Anemia & MDS International Foundation, and American Heart Association grant number 0835085N (to Z.Y.) and from the ELSA U. PARDEE FOUNDATION, American Heart Association, and American Cancer Society Institutional Research Grant #11-053-01-IRG (to C.L.).

References

[1] C.L. Addison, T.O. Daniel, M.D. Burdick, H. Liu, J.E. Ehlert, Y.Y. Xue, L. Buechi, A. Walz, A. Richmond, R.M. Strieter, The CXC chemokine receptor 2, CXCR2, is the putative receptor for ELR+ CXC chemokine-induced angiogenic activity, J. Immunol. 165 (2000) 5269–5277.
[2] R.W. Chapman, J.E. Phillips, R.W. Hipkin, A.K. Curran, D. Lundell, J.S. Fine, CXCR2 antagonists for the treatment of pulmonary disease, Pharmacol. Ther. 121 (2009) 55–68.
[3] H.H. Tsai, E. Frost, V. To, S. Robinson, C. Ffrench-Constant, R. Geertman, R.M. Ransohoff, R.H. Miller, The chemokine receptor CXCR2 controls positioning of oligodendrocyte precursors in developing spinal cord by arresting their migration, Cell 110 (2002) 373–383.
[4] Y. Wu, S. Wang, S.M. Farooq, M.P. Castelvetere, Y. Hou, J.L. Gao, J.V. Navarro, D. Oupicky, F. Sun, C. Li, A chemokine receptor CXCR2 macromolecular complex regulates neutrophil functions in inflammatory diseases, J. Biol. Chem. 287 (2012) 5744–5755.
[5] J. Vandercappellen, J. Van Damme, S. Struyf, The role of CXC chemokines and their receptors in cancer, Cancer Lett. 267 (2008) 226–244.
[6] T. Jamieson, M. Clarke, C.W. Steele, M.S. Samuel, J. Neumann, A. Jung, D. Huels, M.F. Olson, S. Das, R.J. Nibbs, O.J. Sansom, Inhibition of CXCR2 profoundly suppresses inflammation-driven and spontaneous tumorigenesis, J. Clin. Invest. 122 (2012) 3127–3144.
[7] F. Hussain, J. Wang, R. Ahmed, S.K. Guest, E.W. Lam, G. Stamp, M. El-Bahrawy, The expression of IL-8 and IL-8 receptors in pancreatic adenocarcinomas and pancreatic neuroendocrine tumours, Cytokine 49 (2010) 134–140.
[8] A. Li, J. King, A. Moro, M.D. Sugi, D.W. Dawson, J. Kaplan, G. Li, X. Lu, R.M. Strieter, M. Burdick, V.L. Go, H.A. Reber, G. Eibl, O.J. Hines, Overexpression of CXCL5 is associated with poor survival in patients with pancreatic cancer, Am. J. Pathol. 178 (2011) 1340–1349.
[9] S. Wang, Y. Wu, Y. Hou, X. Guan, M.P. Castelvetere, J.J. Oblak, S. Banerjee, T.M. Filtz, F.H. Sarkar, X. Chen, B.P. Jena, C. Li, CXCR2 macromolecular complex in pancreatic cancer: a potential therapeutic target in tumor growth, Transl. Oncol. 6 (2013) 216–225.
[10] M. Miyamoto, Y. Shimizu, K. Okada, Y. Kashii, K. Higuchi, A. Watanabe, Effect of interleukin-8 on production of tumor-associated substances and autocrine growth of human liver and pancreatic cancer cells, Cancer Immunol. Immunother. 47 (1998) 47–57.
[11] H. Takamori, Z.G. Oades, O.C. Hoch, M. Burger, I.U. Schraufstatter, Autocrine growth effect of IL-8 and GROalpha on a human pancreatic cancer cell line, Capan-1, Pancreas 21 (2000) 52–56.
[12] A.C. Magalhaes, H. Dunn, S.S. Ferguson, Regulation of GPCR activity, trafficking and localization by GPCR-interacting proteins, Br. J. Pharmacol. 165 (2012) 1717–1736.
[13] N.F. Neel, M. Barzik, D. Raman, T. Sobolik-Delmaire, J. Sai, A.J. Ham, R.L. Mernaugh, F.B. Gertler, A. Richmond, VASP is a CXCR2-interacting protein that regulates CXCR2-mediated polarization and chemotaxis, J. Cell Sci. 122 (2009) 1882–1894.
[14] J.K. Kim, S. Lim, J. Kim, S. Kim, J.H. Kim, S.H. Ryu, P.G. Suh, Subtype-specific roles of phospholipase C-beta via differential interactions with PDZ domain proteins, Adv. Enzyme Regul. 51 (2011) 138–151.
[15] S. Shenolikar, J.W. Voltz, R. Cunningham, E.J. Weinman, Regulation of ion transport by the NHERF family of PDZ proteins, Physiology (Bethesda) 19 (2004) 362–369.
[16] B.Z. Harris, W.A. Lim, Mechanism and role of PDZ domains in signaling complex assembly, J. Cell Sci. 114 (2001) 3219–3231.
[17] M. Sheng, C. Sala, PDZ domains and the organization of supramolecular complexes, Annu. Rev. Neurosci. 24 (2001) 1–29.
[18] H.J. Lee, J.J. Zheng, PDZ domains and their binding partners: structure, specificity, and modification, Cell Commun. Signal. 8 (2010) 8.
[19] S. Karthikeyan, T. Leung, J.A. Ladias, Structural basis of the Na^+/H^+ exchanger regulatory factor PDZ1 interaction with the carboxyl-terminal region of the cystic fibrosis transmembrane conductance regulator, J. Biol. Chem. 276 (2001) 19683–19686.
[20] R. Tonikian, Y. Zhang, S.L. Sazinsky, B. Currell, J.H. Yeh, B. Reva, H.A. Held, B.A. Appleton, M. Evangelista, Y. Wu, X. Xin, A.C. Chan, S. Seshagiri, L.A. Lasky, C. Sander, C. Boone, G.D. Bader, S.S. Sidhu, A specificity map for the PDZ domain family, PLoS Biol. 6 (2008) e239.
[21] W. Kabsch, Xds, Acta Crystallogr. D Biol. Crystallogr. 66 (2010) 125–132.
[22] A.J. McCoy, R.W. Grosse-Kunstleve, P.D. Adams, M.D. Winn, L.C. Storoni, R.J. Read, Phaser crystallographic software, J. Appl. Crystallogr. 40 (2007) 658–674.
[23] P. Emsley, K. Cowtan, Coot: model-building tools for molecular graphics, Acta Crystallogr. D Biol. Crystallogr. 60 (2004) 2126–2132.
[24] P.D. Adams, P.V. Afonine, G. Bunkoczi, V.B. Chen, I.W. Davis, N. Echols, J.J. Headd, L.W. Hung, G.J. Kapral, R.W. Grosse-Kunstleve, A.J. McCoy, N.W. Moriarty, R. Oeffner, R.J. Read, D.C. Richardson, J.S. Richardson, T.C. Terwilliger, P.H. Zwart, PHENIX: a comprehensive Python-based system for macromolecular structure solution, Acta Crystallogr. D Biol. Crystallogr. 66 (2010) 213–221.
[25] V.B. Chen, W.B. Arendall 3rd, J.J. Headd, D.A. Keedy, R.M. Immormino, G.J. Kapral, L.W. Murray, J.S. Richardson, D.C. Richardson, MolProbity: all-atom structure validation for macromolecular crystallography, Acta Crystallogr. D Biol. Crystallogr. 66 (2010) 12–21.
[26] S.T. Runyon, Y. Zhang, B.A. Appleton, S.L. Sazinsky, P. Wu, B. Pan, C. Wiesmann, N.J. Skelton, S.S. Sidhu, Structural and functional analysis of the PDZ domains of human HtrA1 and HtrA3, Protein Sci. 16 (2007) 2454–2471.
[27] G. Lu, Y. Wu, Y. Jiang, S. Wang, Y. Hou, X. Guan, J. Brunzelle, N. Sirinupong, S. Sheng, C. Li, Z. Yang, Structural insights into neutrophilic migration revealed

by the crystal structure of the chemokine receptor CXCR2 in complex with the first PDZ domain of NHERF1, PLoS One 8 (2013) e76219.
[28] Y. Jiang, G. Lu, L.R. Trescott, Y. Hou, X. Guan, S. Wang, A. Stamenkovich, J. Brunzelle, N. Sirinupong, C. Li, Z. Yang, New conformational state of NHERF1–CXCR2 signaling complex captured by crystal lattice trapping, PLoS One 8 (2013) e81904.
[29] R.A. Cardone, M.R. Greco, M. Capulli, E.J. Weinman, G. Busco, A. Bellizzi, V. Casavola, E. Antelmi, B. Ambruosi, M.E. Dell'Aquila, A. Paradiso, A. Teti, N. Rucci, S.J. Reshkin, NHERF1 acts as a molecular switch to program metastatic behavior and organotropism via its PDZ domains, Mol. Biol. Cell 23 (2012) 2028–2040.
[30] M.A. Larkin, G. Blackshields, N.P. Brown, R. Chenna, P.A. McGettigan, H. McWilliam, F. Valentin, I.M. Wallace, A. Wilm, R. Lopez, J.D. Thompson, T.J. Gibson, D.G. Higgins, Clustal W and Clustal X version 2.0, Bioinformatics 23 (2007) 2947–2948.